

High-order semi-Lagrangian kinetic scheme for compressible turbulence

Dominik Wilde,^{1,2} Andreas Krämer,³ Dirk Reith,^{2,4} and Holger Foysi¹

¹*Department of Mechanical Engineering, University of Siegen,
Paul-Bonatz-Straße 9-11, 57076 Siegen-Weidenau, Germany*

²*Institute of Technology, Resource and Energy-efficient Engineering (TREE),
Bonn-Rhein-Sieg University of Applied Sciences, Grantham-Allee 20, 53757 Sankt Augustin, Germany*

³*Department of Mathematics and Computer Science,
Freie Universität Berlin, Arnimallee 6, 14195 Berlin, Germany*

⁴*Fraunhofer Institute for Algorithms and Scientific Computing (SCAI),
Schloss Birlinghoven, 53754 Sankt Augustin, Germany*

(Dated: December 22, 2024)

Turbulent compressible flows are traditionally simulated using explicit Eulerian time integration applied to the Navier-Stokes equations. However, the associated Courant-Friedrichs-Lowy condition severely restricts the maximum time step size. Exploiting the Lagrangian nature of the Boltzmann equation's material derivative, we now introduce a feasible three-dimensional semi-Lagrangian lattice Boltzmann method (SLLBM), which elegantly circumvents this restriction. Previous lattice Boltzmann methods for compressible flows were mostly restricted to two dimensions due to the enormous number of discrete velocities needed in three dimensions. In contrast, this Rapid Communication demonstrates how cubature rules enhance the SLLBM to yield a three-dimensional velocity set with only 45 discrete velocities. Based on simulations of a compressible Taylor-Green vortex we show that the new method accurately captures shocks or shocklets as well as turbulence in 3D without utilizing additional filtering or stabilizing techniques, even when the time step sizes are up to two orders of magnitude larger compared to simulations in the literature. Our new method therefore enables researchers for the first time to study compressible turbulent flows by a fully explicit scheme, whose range of admissible time step sizes is only dictated by physics, while being decoupled from the spatial discretization.

One major challenge in fluid dynamics is the study of compressible turbulent flows, involving intrinsic as well as variable density compressibility effects [1–7]. Applications range from aviation [8] or astrophysics [9] to the investigation of canonical flows like boundary layers [10], channel flow [11–13], mixing layers [14–18], jets and aeroacoustics [19–21] or shock-turbulence interaction [22], to only mention a few considering the vast literature available. These flows feature both solenoidal and dilatational structures, which constantly interact and possibly cause shock waves [5, 23].

Numerical simulations have become an indispensable tool to understand their physics, and many studies exploring compressible turbulent flows have been conducted using high-order compact finite difference, optimized dispersion-relation preserving schemes [19, 24–30] for the spatial derivatives, often combined with low-dispersion-dissipation Runge-Kutta schemes for time-integration [19, 31, 32]. Although these methods provide accurate results, the time steps are generally small [33], because of the methods' Eulerian time derivatives, which describe how the variables of interest pass through fixed locations in the field. Thus, the admissible time step sizes are tightly linked to spatial resolution. This issue is for many discretizations linked to the Courant-Friedrichs-Lowy (CFL) condition,

$$c\delta_t/\delta_x < \text{CFL}_{\max}, \quad (1)$$

using linear stability theory, relating a characteristic velocity c to the spatial and temporal discretization intervals δ_x and δ_t , respectively (see [34], for example).

Though implicit time integration schemes often provide larger stability domains, their application can be unfeasible for transient problems due to their computational cost. Explicit time integration schemes with scheme-specific CFL_{\max} , in contrast, enforce small time steps δ_t for high flow velocities, typically occurring in many high-speed compressible flows. Another obvious way to circumvent the CFL condition in Eq. (1) is to incorporate Lagrangian time derivatives, which track the motion of the variables of interest moving through the domain. In practice, Semi-Lagrangian (SL) schemes are used instead, which provide a viable alternative to the discretization of Eulerian time derivatives. SL schemes discretize the Lagrangian solution by tracking the trajectories back in time. The prefix “semi” indicates that the trajectories’ end points usually do not coincide with the simulation grid points, necessitating application of an appropriate interpolation scheme. SL methods were successfully incorporated in algorithms solving the Navier-Stokes equations [35], although tracking of the fluid trajectories was often found to be cumbersome, additionally introducing additional errors [36]. The major advantage when using SL schemes in kinetic theory is that the trajectories become *linear*, resulting in cancellation of the tracking error. Consequently, SL schemes were both applied to the Vlasov equation [37–39] and to the Bhatnagar-Gross-Krook (BGK)-Boltzmann equation [40, 41]. Recently, the semi-Lagrangian lattice Boltzmann method (SLLBM) [42, 43] for compressible flows [44] was successfully introduced.

In this Rapid Communication, we significantly advance

the SLLBM for compressible flows by answering how the method can efficiently be extended to three dimensions. Furthermore, we are simultaneously able to increase the time step size by up to two orders of magnitude while retaining stability, giving this approach a decisive edge over previous LBM methods for compressible flows. This is achieved by combining the SLLBM with state-of-the-art cubature rules for the velocity discretization [45, 46]. This combination proves capable of modeling compressible turbulence with time steps that are at least one order of magnitude larger than in standard Eulerian methods and *decouple* the spatial from the temporal discretization.

Semi-Lagrangian lattice Boltzmann method – We start with a critical look at the more specialized lattice Boltzmann method (LBM) [47]. Despite the successes of the standard LBM in the computation of multiphase [48], particle-laden [49], thermal [50], or turbulent flows [51, 52], compressible LBM [53] were overlooked for a relatively long time, but regained attraction during the last decade [54–67].

Let us recall the force-free BGK-Boltzmann equation

$$\frac{\partial f}{\partial t} + \boldsymbol{\xi} \cdot \nabla f = -\frac{1}{\lambda} (f - f^{\text{eq}}), \quad (2)$$

with the continuous distribution function f , the equilibrium distribution function f^{eq} , the particle velocity $\boldsymbol{\xi}$, and the relaxation time λ . To discretize Eq. (2), the original LBM is based on three key principles. First, the equilibrium distribution function f^{eq} is polynomially expanded into a series of Hermite polynomials $\mathcal{H}^{(n)}$, with expansion coefficients being the equilibrium moments $a^{(n),\text{eq}}$ [68],

$$f^{\text{eq},N} \approx \omega(\boldsymbol{\xi}) \sum_{n=0}^N \frac{1}{n!} a^{(n),\text{eq}} \mathcal{H}^{(n)}, \quad (3)$$

N being the expansion order and $\omega(\boldsymbol{\xi})$ the weight function. Second, a Gauß-Hermite quadrature is applied to the unbounded velocity space of the Boltzmann equation, leading to discrete particle velocity sets [68]. The moments are then found by the quadrature

$$a^{(n)} = \int_{-\infty}^{\infty} \omega(\boldsymbol{\xi}) \frac{f}{\omega(\boldsymbol{\xi})} \mathcal{H}^{(n)} d\boldsymbol{\xi} = \sum_{i=0}^{Q-1} f_i \mathcal{H}^{(n)}(\boldsymbol{\xi}_i). \quad (4)$$

with the weighted discrete distribution functions $f_i = w_i f(\boldsymbol{\xi}_i)/\omega(\boldsymbol{\xi}_i)$. The combination of Q discrete particle velocities $\boldsymbol{\xi}_i$ and Q weights w_i , the velocity set, is usually derived by the Gauß-product rule applied to a one-dimensional Gauß-Hermite quadrature. Third, the discrete Boltzmann equation is integrated along characteristics with an inherent Lagrangian discretization of the Boltzmann equation's material derivative to obtain a stable numerical scheme and second-order temporal convergence [69].

Unfortunately, the LBM in its original formulation is mainly restricted to Cartesian grids and velocity discretizations that match the regular lattices. The customary “D2Q9” based on second-order expansion in Eq.

(3) is plagued by a cubic error being proportional to the Mach number. Consequently, compressible simulations demand higher-order discretizations of Eqs. (3) and (4) which render abscissae that reside off-lattice. Utilization of such velocity sets therefore requires an efficient off-lattice Boltzmann solver. Previous Eulerian off-lattice Boltzmann schemes [70–74], like finite difference or finite volume LBM, would be suited in principle. However, they sacrifice the Lagrangian time integration along characteristics. Moreover, their time step is severely restricted by a CFL condition, Eq. (1), with respect to the fast discrete particle velocities.

In contrast, the SLLBM preserves all of the aforementioned key principles of the LBM but it also decisively extends its capabilities. In previous works [42–44] we showed that a high-order interpolation increases the spatial order of the method and nihiliates mass losses. Also, we demonstrated the unconditional stability of the advection step, when incorporating Gauß-Lobatto-Chebyshev nodes for the interpolation up to third order, and that the stability is practically not affected even with fourth order. The flexibility in terms of meshing and velocity sets encouraged us to search for efficient quadrature rules solving the weight function. This research led us to long-established cubature rules [45, 46], i.e. multivariate quadratures, which are heavily used in Kalman filters, e.g. in [75].

The compressible SLLBM uses the established lattice Boltzmann equation with the BGK collision operator [42]

$$h_i(\mathbf{x} + \delta_t \boldsymbol{\xi}_i, t + \delta_t) = h_i(\mathbf{x}, t) - \frac{1}{\tau} (h_i(\mathbf{x}, t) - h_i^{\text{eq}}(\mathbf{x}, t)), \quad (5)$$

with h_i being either f_i or the second distribution function g_i related to the variable heat capacity ratio γ , and the shifted relaxation time $\tau = \lambda + 0.5 = \mu/(\delta_t p) + 0.5$, depending on dynamic viscosity μ and pressure p . The equilibrium distribution function f_i^{eq} is known from Eq. (3) and $g^{\text{eq}} = (2C_v - D)\theta f_i^{\text{eq}}$, with heat capacity at constant volume C_v , number of dimensions D , and relative temperature $\theta = T/T_0$. To adjust the heat conductivity a quasi-equilibrium approach can be applied to Eq. (5) [76]. Density ρ , momentum ρu , and energy E are determined by

$$\rho = \sum_{i=0}^{Q-1} f_i, \quad \rho u = \sum_{i=0}^{Q-1} f_i \boldsymbol{\xi}_i, \quad 2\rho E = \sum_{i=0}^{Q-1} (f_i |\boldsymbol{\xi}_i|^2 + g_i). \quad (6)$$

The integration along characteristics, hidden in Eq. (5), incorporates a second-order temporal error, whose order can be increased by multistep schemes [77]. In standard LBMs, the particle velocities $\boldsymbol{\xi}_i$ in Eq. (5) are designed to end up on one of the neighboring nodes, and the time step size is invariably set to unity for the same purpose. In contrast, the SLLBM's particle distribution functions are still integrated along characteristics, but the departure points may reside offside the grid, i.e. they are off-lattice. To recover the off-lattice values an interpolation is needed. While several interpolation strategies

are possible, we chose a cell-oriented approach, which means that once a departure point's position is identified, the enclosing cell's support points $\hat{f}_{i\Xi j}$ are used for the interpolation

$$\mathbf{f}_i(\mathbf{x}, t) = \sum_{j=1}^{N_j} \hat{f}_{i\Xi j}(t) \psi_{\Xi j}(\mathbf{x}) \quad (7)$$

in cell Ξ and with the interpolation coefficients $\psi_{\Xi j}$, also depicted by Fig. 1 in [42]. For each of the N support points in the simulation, there are Q particle velocities, i.e. there are $N \cdot Q$ departure points to be identified. Therefore, at the beginning of the simulation the path from each support point to the corresponding departure point is tracked through all adjacent cells. Then a sparse matrix Ψ stores the interpolation coefficients $\psi_{\Xi j}$ belonging to the departure point's position; a pseudo-algorithm is presented in [43]. The actual streaming step is expressed as a matrix-vector multiplication

$$\mathbf{f}_i(t + \delta_t) = \Psi_i \mathbf{f}_i(t), \quad (8)$$

whereas the collision step remains local.

Cubature-based velocity sets – The discretization of the velocity space is a key principle for any simulation with the lattice Boltzmann method. If a quadrature is applied to obey the second key principle including Eq. (4), it must be suited to integrate the weight function $\exp(-x^2)$, and it has to be of ninth degree to enable compressible flow simulations [78]. A prominent method to derive two- and three-dimensional velocity sets is the Gauß-product rule applied to a one-dimensional quadrature. Application to the one-dimensional degree-nine Gauß-Hermite quadrature delivers a two-dimensional D2Q25 off-lattice velocity set with 25 abscissae, which we used for previous work [44]. Due to its structure, this velocity set is infeasible for standard on-lattice streaming but perfectly suited for the SLLBM. For the results in this work we made use of velocity sets, which were derived by cubature rules [45, 46], exhibiting the same degree of precision, but consisting of fewer support points to lower computational cost. In two dimensions we employed a degree-nine D2Q19 velocity set with 19 abscissae [79]. In three dimensions, the Gauß-product rule led to noncompetitive 125 abscissae for a three-dimensional degree-nine D3Q125 velocity set. Therefore, we successfully identified and implemented a degree-nine D3Q45 velocity set with only 45 components, which fulfills all requirements in terms of symmetry. The D3Q45 was derived by a cubature rule after Konyaev [80] and has recently been picked up again by van Zandt in the cubature literature [81]. The resulting discrete velocities are shown in Fig. 1, whereas weights and abscissae of the D2Q19 and D3Q45 are listed in the Appendix. The research for even compacter cubature rules is still ongoing, so that future degree-nine velocity sets will possibly be even more efficient.

Temporally underresolved Sod shock tube – First, we simulate a Sod shock tube with the configuration detailed

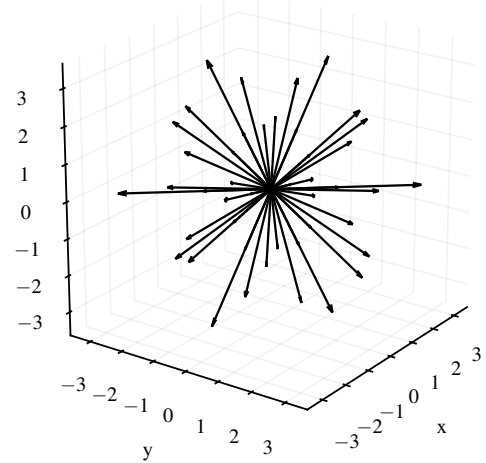


FIG. 1. Three-dimensional D3Q45 velocity set with 45 abscissae, derived by a degree-nine cubature rule originally by Konyaev [80]

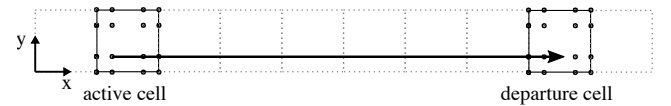


FIG. 2. Exemplary departure point location for the Sod shock tube configuration in this article with 2000 cells. The path of the longest abscissa of the 2D velocity set D2Q19 is shown. Starting from the current cell, the abscissa's path linearly traverses six contiguous cells and locates the departure point in the seventh cell. A 3rd-order polynomial interpolation using the cell-local Gauß-Lobatto-Chebyshev support points is applied to reconstruct the distribution function value.

in [44] to illustrate the large range of time step sizes accessible to the SLLBM, using a pressure ratio of 10:1 and a viscosity of $\mu = 7 \cdot 10^{-4}$. The domain $x \in [0, 1]$ was discretized using 2000 cells at third polynomial order, i.e. 6000 grid points in x direction.

Despite this fine spatial resolution that we only chose for demonstration purposes, the time step size was set to $\delta_t = 0.001$, such that the solution at $t = 0.1$ was reached by performing only 100 time steps. The same configuration simulated by a spectral-element discontinuous Galerkin solver for the streaming step [43, 72] produced nearly identical results, but required 1154 time steps with an explicit exponential time integrator [82] and 2200 time steps with the more common fourth-order Runge-Kutta method. As the distance of the departure points from the active nodes is proportional to the time step size (Eq. 5), the departure points of the SLLBM were located up to seven cells away. The trajectory is shown in Fig. 2 for an exemplary departure point. It is obvious, that the CFL restriction of explicit Eulerian solvers prohibits the exchange of information crossing multiple cells. This property is of special interest in case of simulations with body-fitted meshes, where the spatial extent

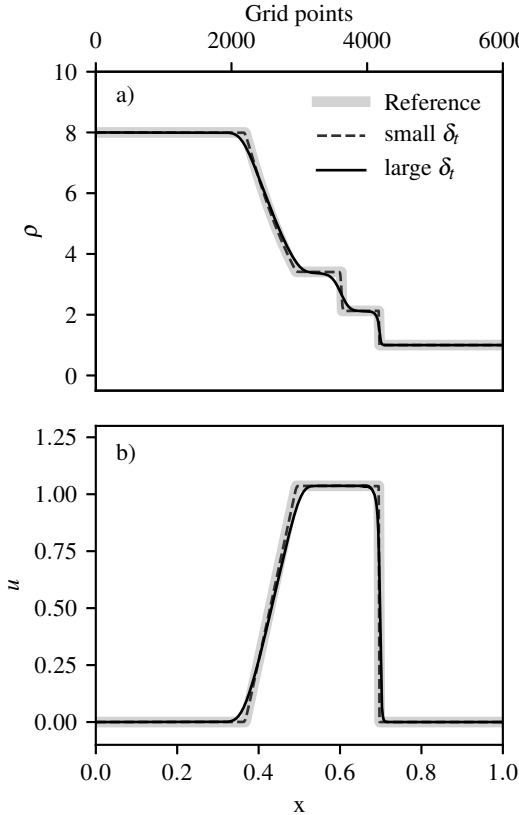


FIG. 3. a) Density b) velocity of Sod shock tube simulation using SLLBM at time $t = 0.1$, which is reached after only 100 time steps (large δ_t), despite the fine spatial resolution of 6000 grid points. “Small δ_t ” simulated with 2000 time steps.

of the smallest cells usually dictates the time step size of the whole simulation. As opposed to Eulerian solvers, the maximum stable time step size in the SLLBM is proportional only to the viscosity and not dictated by the mesh size. On top of that, when doubling the number of cells the number of SLLBM time steps can still be kept constant, whereas it inevitably doubles for the explicit discontinuous Galerkin solver. Fig. 3 shows that the SLLBM accurately traces the shock front despite the extremely large time step. For a smaller time step size of $\delta_t = 0.0005$ and viscosity of $\mu = 10^{-5}$ the simulation results perfectly matched the inviscid reference solution.

Compressible turbulence simulations – To show that the SLLBM captures the intricate interactions between turbulent and compressible features including shocklets, the compressible three-dimensional Taylor-Green vortex flow was simulated. In comparison to forced or decaying isotropic turbulence, this test case enables a standardized initialization and thus an easier and more objective comparison. This flow was thoroughly studied by Peng and Yang [83] using a Reynolds number of $Re = 400$. The original work used a compact eighth-order finite difference scheme [24] to discretize the convective terms in the Navier-Stokes equation in combination with a seventh-order weighted essentially non-oscillatory

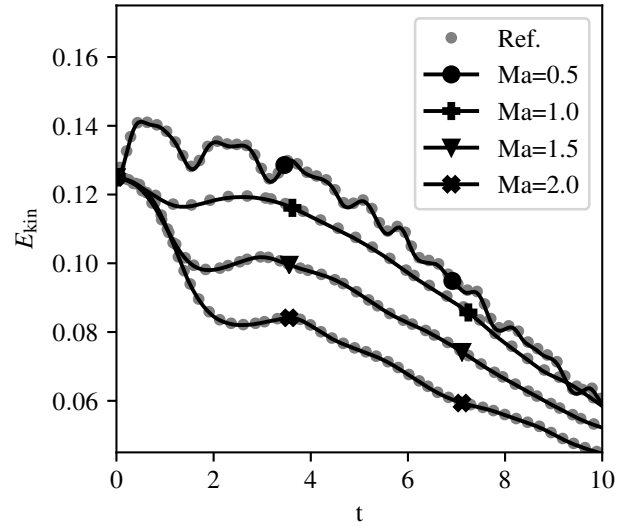


FIG. 4. Kinetic energy over time of the compressible 3D Taylor-Green vortex. Simulations by the SLLBM with the D3Q45 velocity set shown in Fig. 1. Reference from [83].

(WENO) scheme. The present compressible SLLBM uses fourth-order polynomials for the equilibrium (Eq. (3)) and for the interpolation (Eq. (7)), *without utilizing additional filtering or stabilizing techniques*. Moreover, to satisfy the CFL condition, the original work applied a time step size of $\delta_t = 0.0005$, whereas the SLLBM was capable to utilize time step sizes two orders of magnitude larger: $\delta_t = 0.017$ for Mach number $Ma = 0.5$, $\delta_t = 0.033$ for $Ma = 1.0$, $\delta_t = 0.018$ for $Ma = 1.5$, and $\delta_t = 0.012$ for $Ma = 2.0$. The spatial resolution was $N = 256^3$. Fig. 4 depicts the kinetic energy over time for all Mach numbers, which accurately follows the reference solution despite the coarse temporal discretization. Additionally, as shown in the Appendix for $Re = 100$ we were able to stably simulate the given test case for Mach numbers $Ma = 2.5$ and $Ma = 3.0$, which indicates that the applicability of the numerical method is not limited to weakly supersonic flows. Own future work will therefore explore the capabilities of the SLLBM for other supersonic flows, involving the well known compressible channel flows [12] and jets [21].

Conclusion The compressible SLLBM introduced in this communication offers significant advantages compared to other methods. Because of its linear characteristics, the LBM perfectly suits SL schemes. Consequently, the SLLBM allows very large time steps sizes while not being restricted by the customary CFL condition. Although the presented SLLBM is a fourth-order spatial method and accurately captures shocks as well as turbulence, no stabilization or filtering were required for the presented test cases. Due to these unique features, the cubature-based fully explicit SLLBM presented in this communication enables researchers for the first time, to the best of our knowledge, to perform compressible tur-

bulence simulations, in which the admissible time step sizes are decoupled from the spatial discretization, opening a new field of affordable simulations for compressible turbulent flows.

ACKNOWLEDGMENTS

This work was supported by the German Ministry of Education and Research and the Ministry for Culture and Science North Rhine-Westfalia (research grant 13FH156IN6). D.W. is supported by German Research Foundation (DFG) project FO 674/17-1. D.W. and A.K. contributed equally to this work.

Appendix A: Three-dimensional compressible Taylor-Green vortex

On the triply-periodic domain $[0, 2\pi]^3$, the initial conditions with constant temperature initial condition (CTIC) are given as follows

$$\begin{aligned} u_1(x_1, x_2, x_3, t = 0) &= \sin x_1 \cos x_2 \cos x_3, \\ u_2(x_1, x_2, x_3, t = 0) &= -\cos x_1 \sin x_2 \cos x_3, \\ u_3(x_1, x_2, x_3, t = 0) &= 0, \\ \rho(x_1, x_2, x_3, t = 0) &= 1 + \frac{\mathcal{C}}{16} [\cos(2x_1) + \cos(2x_2)] [\cos(2x_3 + 2)], \\ T(x_1, x_2, x_3, t = 0) &= 1 \end{aligned}$$

with velocities \mathbf{u} , density ρ , Mach number Ma , and temperature T . The numerator \mathcal{C} can either be $\mathcal{C} = 1$ or $\mathcal{C} = \text{Ma}^2$. All results in the present article were obtained with $\mathcal{C} = 1$. The Reynolds number is defined as $Re = 1/\nu_\infty$, with the kinematic viscosity ν at $T = 1$. The Prandtl number is $Pr = 0.7$; the heat capacity ratio is $\gamma = 1.4$. The dynamic viscosity $\mu = \nu\rho$ obeys the Sutherland law

$$\mu = \frac{1.4042T^{1.5}}{T + 0.40417}\mu_\infty. \quad (\text{A1})$$

1. Additional results for $\text{Re}=100$, $\text{Re}=400$, and $\text{Re}=1600$

Fig. 5 plots the kinetic energies over time of the three-dimensional compressible Taylor-Green vortex for additional Reynolds numbers and Mach numbers at resolution $N = 128^3$.

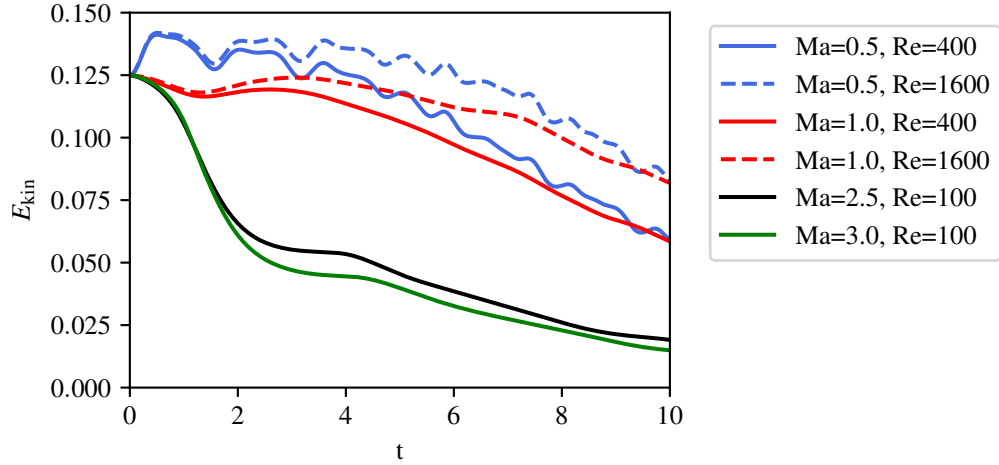


FIG. 5. Additional results for the compressible three-dimensional Taylor-Green vortex. The kinetic energy over time is shown for different configurations.

Appendix B: D2Q19 velocity set

w	ξ_x	ξ_y
0.3168437267921905	0.0	0.0
0.10558878375062891	0.0	-1.4869982213169028
0.10558878375062891	0.0	1.4869982213169028
0.1024247123210936	1.367469636752619	0.775196278121181
0.1024247123210936	-1.367469636752619	0.775196278121181
0.1024247123210936	1.367469636752619	-0.775196278121181
0.1024247123210936	-1.367469636752619	-0.775196278121181
0.00953510698543825	1.105629214668943	2.5175897644357486
0.00953510698543825	-1.105629214668943	2.5175897644357486
0.00953510698543825	-1.105629214668943	-2.5175897644357486
0.00953510698543825	1.105629214668943	-2.5175897644357486
0.006865104210104631	2.9213306655318734	0.0
0.006865104210104631	-2.9213306655318734	0.0
0.002405335328939458	2.6987507639352253	1.8663975507141328
0.002405335328939458	2.6987507639352253	-1.8663975507141328
0.002405335328939458	-2.6987507639352253	1.8663975507141328
0.002405335328939458	-2.6987507639352253	-1.8663975507141328
0.0003939393722285871	0.0	-3.8358342053914734
0.0003939393722285871	0.0	3.8358342053914734

lattice constant $c_s = 1$

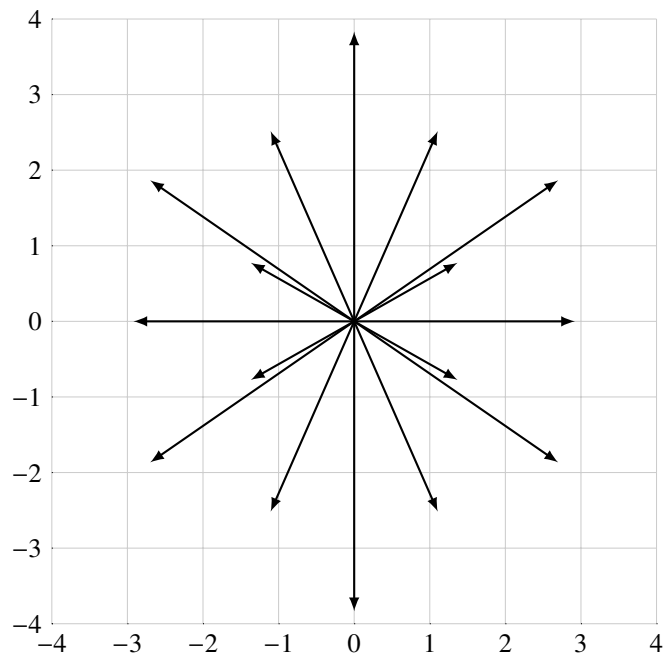


FIG. 6. D2Q19 velocity set

Appendix C: D3Q45 velocity set

w	e_x	e_y	e_z
0.20740740740740618	0.0	0.0	0.0
0.05787037037037047	-0.06386083877343968	1.2239121278243665	1.2239121278243665
0.05787037037037047	1.2239121278243665	-0.06386083877343968	1.2239121278243665
0.05787037037037047	1.2239121278243665	1.2239121278243665	-0.06386083877343968
0.05787037037037047	0.06386083877343968	-1.2239121278243665	-1.2239121278243665
0.05787037037037047	-1.2239121278243665	-1.2239121278243665	0.06386083877343968
0.05787037037037047	-1.2239121278243665	0.06386083877343968	-1.2239121278243665
0.05787037037037047	-1.5766994272507744	0.5069610024977665	0.5069610024977665
0.05787037037037047	1.5766994272507744	-0.5069610024977665	-0.5069610024977665
0.05787037037037047	0.5069610024977665	0.5069610024977665	-1.5766994272507744
0.05787037037037047	-0.5069610024977665	-0.5069610024977665	1.5766994272507744
0.05787037037037047	-0.5069610024977665	1.5766994272507744	-0.5069610024977665
0.05787037037037047	0.5069610024977665	-1.5766994272507744	0.5069610024977665
0.00462962962962958	-2.403092127540177	-0.8892242114059369	1.5602655313772367
0.00462962962962958	2.403092127540177	0.8892242114059369	-1.5602655313772367
0.00462962962962958	-0.8892242114059369	-2.403092127540177	1.5602655313772367
0.00462962962962958	0.8892242114059369	2.403092127540177	-1.5602655313772367
0.00462962962962958	-0.8892242114059369	1.5602655313772367	-2.403092127540177
0.00462962962962958	-2.403092127540177	1.5602655313772367	-0.8892242114059369
0.00462962962962958	-1.5602655313772367	0.8892242114059369	2.403092127540177
0.00462962962962958	-1.5602655313772367	2.403092127540177	0.8892242114059369
0.00462962962962958	0.8892242114059369	-1.5602655313772367	2.403092127540177
0.00462962962962958	1.5602655313772367	-0.8892242114059369	-2.403092127540177
0.00462962962962958	2.403092127540177	-1.5602655313772367	0.8892242114059369
0.00462962962962958	1.5602655313772367	-2.403092127540177	-0.8892242114059369
0.00462962962962958	0.4744978678080795	0.4744978678080795	2.9239876105912574
0.00462962962962958	0.4744978678080795	2.9239876105912574	0.4744978678080795
0.00462962962962958	2.9239876105912574	0.4744978678080795	0.4744978678080795
0.00462962962962958	-0.4744978678080795	-0.4744978678080795	-2.9239876105912574
0.00462962962962958	-0.4744978678080795	-2.9239876105912574	-0.4744978678080795
0.00462962962962958	-2.9239876105912574	-0.4744978678080795	-0.4744978678080795
0.00462962962962958	1.7320508075688787	1.7320508075688787	1.7320508075688787
0.00462962962962958	-1.7320508075688787	-1.7320508075688787	-1.7320508075688787
0.0004629629629629939	-2.7367507163016924	0.14279717659756475	-2.7367507163016924
0.0004629629629629939	0.14279717659756475	-2.7367507163016924	-2.7367507163016924
0.0004629629629629939	2.7367507163016924	2.7367507163016924	-0.14279717659756475
0.0004629629629629939	2.7367507163016924	-0.14279717659756475	2.7367507163016924
0.0004629629629629939	-0.14279717659756475	2.7367507163016924	2.7367507163016924
0.0004629629629629939	-2.7367507163016924	-2.7367507163016924	0.14279717659756475
0.0004629629629629939	-3.5256070994177073	1.1335992635264445	1.1335992635264445
0.0004629629629629939	1.1335992635264445	-3.5256070994177073	1.1335992635264445
0.0004629629629629939	-1.1335992635264445	3.5256070994177073	-1.1335992635264445
0.0004629629629629939	3.5256070994177073	-1.1335992635264445	-1.1335992635264445
0.0004629629629629939	1.1335992635264445	1.1335992635264445	-3.5256070994177073
0.0004629629629629939	-1.1335992635264445	-1.1335992635264445	3.5256070994177073

lattice constant $c_s = 1$

- [1] S. K. Lele, Compressibility effects on turbulence, *Annual Review of Fluid Mechanics* **26**, 211 (1994).
- [2] P. Chassaing, R. Antonia, F. Anselmet, L. Joly, and S. Sarkar, *Variable Density Fluid Turbulence* (Kluwer Academic Publishers, 2002).
- [3] L. Veynante, D. Vervisch, Turbulent combustion modelling, *Prog. Energy Combust. Sci.* **30**, 193 (2002).
- [4] A. J. Smits and J. P. Dussauge, *Turbulent Shear Layers in Supersonic Flow: Second Edition* (Springer, 2006).
- [5] E. Garnier, N. Adams, and P. Sagaut, *LES for compressible flows* (Springer, 2009).

ible flows (Springer, 2009).

[6] S. Pirozzoli, Numerical Methods for High-Speed Flows, *Annu. Rev. Fluid Mech.* **43**, 163 (2011).

[7] T. B. Gatski and J.-P. Bonnet, *Compressibility, Turbulence and High Speed Flow* (Academic Press, 2013).

[8] R. Sharman and T. Lane, *Aviation turbulence: Processes, detection, prediction* (Springer, 2016) pp. 1–523.

[9] M. M. M. Low and R. S. Klessen, Control of star formation by supersonic turbulence, *Rev. Mod. Phys.* **76**, 125 (2004), 0301093 [astro-ph].

[10] H. H. Fernholz and P. J. Finley, *A critical compilation of compressible turbulent boundary layer data* (AGAR-Dograph 223, 1976).

[11] P. Huang, G. Coleman, and P. Bradshaw, Compressible turbulent channel flows: DNS results and modelling, *J. Fluid Mech.* **305**, 185 (1995).

[12] H. Foysi, S. Sarkar, and R. Friedrich, Compressibility Effects and Turbulence Scalings in Supersonic Channel Flow, *J. Fluid Mech.* **509**, 207 (2004).

[13] S. Ghosh, H. Foysi, and R. Friedrich, Compressible turbulent channel and pipe flow: similarities and differences, *J. Fluid Mech.* **648**, 155 (2010).

[14] P. Bradshaw, Compressible turbulent shear layers, *Ann. Rev. Fluid Mech.* **21**, 926 (1977).

[15] D. W. Bogdanoff, Compressibility effects in turbulent shear layers, *AIAA Journal* **21**, 926 (1983).

[16] A. W. Vreman, N. D. Sandham, and K. H. Luo, Compressible mixing layer growth rate and turbulence characteristics, *J. Fluid Mech.* **320**, 235 (1996).

[17] H. Foysi and S. Sarkar, The compressible mixing layer: an LES study, *Theoretical and Computational Fluid Dynamics* **24**, 565 (2010).

[18] K. V. Matsuno and S. K. Lele, Compressibility effects in high speed turbulent shear layers - revisited, *AIAA 2020-0573, AIAA SciTech 2020 Forum* (2020).

[19] T. Colonius and S. Lele, Computational aeroacoustics: progress on nonlinear problems of sound generation., *Progr. Aerosp. Sc.* **40**, 345 (2004).

[20] D. Bodony and S. Lele, Review of the current status of jet noise predictions using large-eddy simulation., *AIAA, AIAA-2006-0468* (2006).

[21] H. Foysi, M. Mellado, and S. Sarkar, Simulation and comparison of variable density round and plane jets., *International Journal of Heat and Fluid Flow* **31**, 307 (2010).

[22] S. K. Lele and J. Larsson, Shock-turbulence interaction: What we know and what we can learn from peta-scale simulations, *J. Phys. Conf. Ser.* **180**, 012032 (2009).

[23] S. Lee, S. K. Lele, and P. Moin, Eddy shocklets in decaying compressible turbulence, *Phys. Fluids A Fluid Dyn.* **3**, 657 (1991).

[24] S. K. Lele, Compact finite difference schemes with spectral-like resolution, *J. Comput. Phys.* **103**, 16 (1992).

[25] C. K. Tam and J. C. Webb, Dispersion-relation-preserving finite difference schemes for computational acoustics, *J. Comput. Phys.* **107**, 262 (1993).

[26] N. A. Adams and K. Shariff, A high-resolution hybrid compact-eno scheme for shock-turbulence interaction problems, *J. Comput. Phys.* **127**(1) (1996).

[27] J. A. Ekaterinaris, Implicit, High-Resolution, Compact Schemes for Gas Dynamics and Aeroacoustics, *J. Comput. Phys.* **156**, 272 (1999).

[28] T. K. Sengupta, G. Ganeriwal, and S. De, Analysis of central and upwind compact schemes, *J. Comput. Phys.* **192**, 677 (2003).

[29] C. Bogey and C. Bailly, A family of low dispersive and low dissipative explicit schemes for flow and noise computations, *J. Comput. Phys.* **194**, 194 (2004).

[30] J. Wang, L. P. Wang, Z. Xiao, Y. Shi, and S. Chen, A hybrid numerical simulation of isotropic compressible turbulence, *J. Comput. Phys.* **229**, 5257 (2010).

[31] F. Hu, M. Hussaini, and J. Manthey, Low-dissipation and lowdispersion runge–kutta schemes for computational acoustics, *J. Comput. Phys.* **124**, 177 (1996).

[32] J. Berland, C. Bogey, and C. Bailly, *Low-dissipation and low-dispersion fourth-order Runge-Kutta algorithm.*, Vol. 35 (Comput. Fluids, 2006) pp. 1459–1463.

[33] N. Kwatra, J. Su, J. T. Grétarsson, and R. Fedkiw, A method for avoiding the acoustic time step restriction in compressible flow, *J. Comput. Phys.* **10.1016/j.jcp.2009.02.027** (2009).

[34] B. Müller, Linear Stability Condition for Explicit Runge-Kutta Methods to Solve the Compressible Navier-Stokes Equations, *Math. Models Methods Appl. Sci.* **12**, 139 (1990).

[35] D. Xiu and G. E. Karniadakis, A semi-Lagrangian high-order method for Navier-Stokes equations, *J. Comput. Phys.* **172**, 658 (2001).

[36] E. Celledoni, B. K. Kometa, and O. Verdier, High Order Semi-Lagrangian Methods for the Incompressible Navier–Stokes Equations, *J. of Sci. Computing* **66**, 91 (2016), 1207.5147.

[37] E. Sonnendrücker, J. Roche, P. Bertrand, and A. Ghizzo, The Semi-Lagrangian Method for the Numerical Resolution of the Vlasov Equation, *J. Comput. Phys.* **149**, 201 (1999).

[38] N. Crouseilles, M. Mehrenberger, and E. Sonnendrücker, Conservative semi-Lagrangian schemes for Vlasov equations, *J. Comput. Phys.* **229**, 1927 (2010).

[39] J. M. Qiu and A. Christlieb, A conservative high order semi-Lagrangian WENO method for the Vlasov equation, *J. Comput. Phys.* **229**, 1130 (2010).

[40] G. Russo, P. Santagati, and S. B. Yun, Convergence of a semi-Lagrangian scheme for the BGK model of the Boltzmann equation, *SIAM J. Num. Analysis* **50**, 1111 (2012).

[41] M. Groppi, G. Russo, and G. Stracquadanio, High order semi-lagrangian methods for the bgk equation (2014), arXiv:1411.7929 [math.NA].

[42] A. Krämer, K. Küllmer, D. Reith, W. Joppich, and H. Foysi, Semi-Lagrangian off-lattice Boltzmann method for weakly compressible flows, *Phys. Rev. E* **95** (2017).

[43] A. Krämer, D. Wilde, K. Küllmer, D. Reith, H. Foysi, and W. Joppich, Lattice Boltzmann simulations on irregular grids: Introduction of the NATriuM library, *Comput. Math. with Appl.* **79**, 34 (2020).

[44] D. Wilde, A. Krämer, D. Reith, and H. Foysi, Semi-Lagrangian lattice Boltzmann method for compressible flows, *Phys. Rev. E* **101**, 1 (2020), 1910.13918.

[45] A. H. Stroud, Approximate Calculation of Multiple Integrals, *Math. Comput.* **10.2307/2005635** (1973).

[46] R. Cools, An encyclopaedia of cubature formulas, *Journal of Complexity* **19**, 445 (2003), oberwolfach Special Issue.

[47] T. Krüger, H. Kusumaatmaja, A. Kuzmin, O. Shardt, G. Silva, and E. M. Viggen, *The lattice Boltzmann method: Principles and practice* (Springer Nature, 2017).

[48] L. Chen, Q. Kang, Y. Mu, Y. L. He, and W. Q. Tao, A critical review of the pseudopotential multiphase lattice Boltzmann model: Methods and applications, *Int. J. Heat and Mass Transfer* **76**, 210 (2014).

[49] L. P. Wang, C. Peng, Z. Guo, and Z. Yu, Lattice Boltzmann simulation of particle-laden turbulent channel flow, *Comput. Fluids* **124**, 226 (2016).

[50] Y. Peng, C. Shu, and Y. T. Chew, Simplified thermal lattice Boltzmann model for incompressible thermal flows, *Phys. Rev. E* **68**, 8 (2003).

[51] M. Geier, M. Schönherr, A. Pasquali, and M. Krafczyk, The cumulant lattice Boltzmann equation in three dimensions: Theory and validation, *Comp. and Math. with Appl.* **70**, 507 (2015).

[52] B. Dorschner, F. Bösch, S. S. Chikatamarla, K. Boulouchos, and I. V. Karlin, Entropic multi-relaxation time lattice Boltzmann model for complex flows, *J. Fluid Mech.* **801**, 623 (2016).

[53] F. J. Alexander, H. Chen, S. Chen, and G. D. Doolen, Lattice Boltzmann model for compressible fluids, *Phys. Rev. A* **46**, 1967 (1992).

[54] N. Frapolli, S. S. Chikatamarla, and I. V. Karlin, Entropic lattice Boltzmann model for compressible flows, *Phys. Rev. E* **92**, 061301 (2015).

[55] N. Frapolli, S. S. Chikatamarla, and I. V. Karlin, Lattice Kinetic Theory in a Comoving Galilean Reference Frame, *Phys. Rev. Lett.* **117**, 10604 (2016).

[56] N. Frapolli, S. S. Chikatamarla, and I. V. Karlin, Entropic lattice Boltzmann model for gas dynamics: Theory, boundary conditions, and implementation, *Phys. Rev. E* **93**, 063302 (2016).

[57] Y. Feng, P. Sagaut, and W. Q. Tao, A compressible lattice Boltzmann finite volume model for high subsonic and transonic flows on regular lattices, *Comput. Fluids* **131**, 45 (2016).

[58] C. Coreixas, G. Wissocq, G. Puigt, J. F. Boussuge, and P. Sagaut, Recursive regularization step for high-order lattice Boltzmann methods, *Phys. Rev. E* **96** (2017).

[59] M. Atif, M. Namburi, and S. Ansumali, Higher-order lattice Boltzmann model for thermohydrodynamics, *Phys. Rev. E* **98**, 053311 (2018).

[60] B. Dorschner, F. Bösch, and I. V. Karlin, Particles on Demand for Kinetic Theory, *Phys. Rev. Lett.* **121**, 130602 (2018).

[61] Y. Feng, P. Boivin, J. Jacob, and P. Sagaut, Hybrid recursive regularized thermal lattice Boltzmann model for high subsonic compressible flows, *J. Comput. Phys.* **394**, 82 (2019).

[62] S. A. Hosseini, C. Coreixas, N. Darabiha, and D. Thévenin, Extensive analysis of the lattice Boltzmann method on shifted stencils, *Phys. Review E* **100**, 1 (2019).

[63] M. H. Saadat, F. Bösch, and I. V. Karlin, Lattice Boltzmann model for compressible flows on standard lattices: Variable Prandtl number and adiabatic exponent, *Phys. Rev. E* **99**, 013306 (2019).

[64] M. H. Saadat, F. Bösch, and I. V. Karlin, Semi-Lagrangian lattice Boltzmann model for compressible flows on unstructured meshes, *Phys. Rev. E* **101**, 23311 (2020).

[65] J. Latt, C. Coreixas, J. Beny, and A. Parmigiani, Efficient supersonic flow simulations using lattice Boltzmann methods based on numerical equilibria, *Philos. Trans. R. Soc. A Math. Phys. Eng. Sci.* **378**, 20190559 (2020).

[66] G. Farag, S. Zhao, T. Coratger, P. Boivin, G. Chiavassa, and P. Sagaut, A pressure-based regularized lattice Boltzmann method for the simulation of compressible flows, *Phys. Fluids* **32**, 10.1063/5.0011839 (2020).

[67] C. Coreixas and J. Latt, Compressible lattice boltzmann methods with adaptive velocity stencils: An interpolation-free formulation, *Physics of Fluids* **32**, 116102 (2020), <https://doi.org/10.1063/5.0027986>.

[68] X. Shan and X. He, Discretization of the velocity space in the solution of the Boltzmann equation, *Phys. Rev. Lett.* **80**, 65 (1998), 9712001 [comp-gas].

[69] X. He, S. Chen, and G. D. Doolen, A Novel Thermal Model for the Lattice Boltzmann Method in Incompressible Limit, *J. Comput. Phys.* **146**, 282 (1998).

[70] A. Bardow, I. V. Karlin, and A. A. Gusev, General characteristic-based algorithm for off-lattice Boltzmann simulations, *Europhys. Lett.* **75**, 434 (2006).

[71] T. Lee and C.-L. L. Lin, An Eulerian description of the streaming process in the lattice Boltzmann equation, *J. Comput. Phys.* **185**, 445 (2003).

[72] M. Min and T. Lee, A spectral-element discontinuous Galerkin lattice Boltzmann method for nearly incompressible flows, *J. Comput. Phys.* **230**, 245 (2011).

[73] Z. Guo, K. Xu, and R. Wang, Discrete unified gas kinetic scheme for all Knudsen number flows: low-speed isothermal case, *Phys. Rev. E* **88**, 33305 (2013).

[74] Z. Guo, R. Wang, and K. Xu, Discrete unified gas kinetic scheme for all Knudsen number flows: II. Compressible case, *Phys. Rev. E* **91**, 033313 (2014), 1406.5668.

[75] I. Arasaratnam and S. Haykin, Cubature Kalman Filters, *IEEE Trans. on Automatic Control* **54**, 1254 (2009).

[76] C. Thantanapally, S. Singh, D. V. Patil, S. Succi, and S. Ansumali, Quasiequilibrium lattice Boltzmann models with tunable Prandtl number for incompressible hydrodynamics, *International Journal of Modern Physics C* **24**, 1340004 (2013).

[77] D. Wilde, A. Krämer, K. Küller, H. Foysi, and D. Reith, Multistep lattice Boltzmann methods: Theory and applications, *International Journal for Numerical Methods in Fluids* **90**, 156 (2019).

[78] X. Shan, X. F. Yuan, and H. Chen, Kinetic theory representation of hydrodynamics: A way beyond the Navier-Stokes equation, *J. Fluid Mech.* **550**, 413 (2006).

[79] A. Haegemans and R. Piessens, Construction of cubature formulas of degree seven and nine symmetric planar regions, using orthogonal polynomials, *SIAM J. on Num. Analys.* **14**, 492 (1977), <https://doi.org/10.1137/0714029>.

[80] S. Konyaev, Ninth-order quadrature formulas invariant with respect to the icosahedral group, in *Doklady Akademii Nauk*, Vol. 233 (Russ. Acad. of Sci., 1977) pp. 784–787.

[81] J. R. Van Zandt, Efficient cubature rules, *ETNA - Electron. Trans. Numer. Anal.* **51**, 219 (2019).

[82] K. C. Uga, M. Min, T. Lee, and P. F. Fischer, Spectral-element discontinuous galerkin lattice boltzmann simulation of flow past two cylinders in tandem with an exponential time integrator, *Comp. and Math. with Appl.* **65**, 239 (2013).

[83] N. Peng and Y. Yang, Effects of the Mach number on the evolution of vortex-surface fields in compressible Taylor-Green flows, *Physical Review Fluids* **3**, 1 (2018).